

PHYSIOCHEMICAL PROPERTIES OF TIN OXIDE THIN FILMS DEPOSITED BY SPRAY PYROLYSIS

V. JANAKIRAMAN^a, V. TAMILNAYAGAM^b, R. S. SUNDARARAJAN^a,
S. SIVABALAN^c, B. SATHYASEELAN^{d*}

^a*PG & Research Department of Physics, Government Arts College (Autonomous), Kumbakonam 612002, Tamilnadu, India (Affiliated to Bharathidasan University, Tiruchirappalli, Tamilnadu, India).*

^b*Department of Physics, A.P.A. College of Arts & Culture, Palani, Dindigul, Tamilnadu, India*

^c*Department of Physics, T.B.M.L. College, Porayar 609307, Tamilnadu, India*

^d*Department of Physics, University College of Engineering Arni (A Constituent College of Anna University Chennai) Arni 632326, Tamil Nadu, India*

In this article, tin oxide film is deposited onto glass substrates at 350°C by spray pyrolysis technique. The nature of nanoparticles is investigated using X-ray diffraction, UV-visible spectroscopy, and Fourier transforms infrared spectra. XRD studies are shown that the thin film orientations along (110), (101), (200), (211), (220), (310), (301), and (321) planes. The phase structure is polycrystalline with tetragonal rutile. The average crystallite sizes are determined. Field emission scanning electron microscopy analysis shows that SnO₂ thin film with irregular grains and irregular shapes was found. A Fourier transform infrared spectra characteristics for pure SnO₂ thin films explains various vibrational assignment modes. Energy dispersive spectroscopy analysis confirms the elements of deposited thin films on the glass substrate. UV visible absorption spectra show that the band gap of SnO₂ thin film is 3.57 eV. The SnO₂ thin films are prepared using a simple and economical technique with the advantage that they are used for optoelectronic devices and gas sensor applications.

Keywords: SnO₂ thin films, Spray pyrolysis, Band gap, Gas sensors

(Received April 18, 2020; Accepted August 20, 2020)

1. Introduction

Transparent conductive oxide (TCO) thin films are considered as the most significant interest owing to their unique potential application in gas sensors and optoelectronic devices. SnO₂ is an n-type semiconductor material with a tetragonal rutile crystal structure with lattice parameters of $a = b = 4.737 \text{ \AA}$ and $c = 3.186 \text{ \AA}$ and a wide band gap of 3.6–3.97 eV¹. Tin oxide (SnO₂) is also a unique property of the low electrical resistance and high optical transparency, which has found to be various kinds of technical applications, such as gas sensors², transparent electrodes³, optoelectronic devices⁴, piezoelectric devices⁵, photocatalysts⁶, dye based solar cells⁷, thin-film coolers^{8,9} etc. Tin oxide thin film has the most investigated oxygen deficiencies because of their remarkable properties such as high conductivity. The formation energy of oxygen vacancies and tin interstitials in SnO₂ is very low. Therefore, these defects form readily, which explains the high conductivity of pure, but nonstoichiometric SnO₂¹⁰. Pure SnO₂ thin films were prepared using several chemical and physical methods such as spray pyrolysis^{11–13}, sol-gel process^{14,15}, chemical vapor deposition¹⁶, sputtering¹⁷, and pulsed laser deposition¹⁸. Of these methods, spray pyrolysis technique is simple and low cost. Moreover, the deposition rate and the thickness of the films can be easily controlled over by a wide range by changing the spray parameters. This technique involves a simple technology in which an ionic solution is sprayed over heated substrates. Even though a number of tin salts are available for this purpose, the most suitable one must have the characteristics that the decomposition temperature is not very high, the decomposition reaction

* Corresponding authors: bsseelan03@gmail.com

leading to the formation of SnO_2 is thermodynamically feasible, and no residue of the reactants is left behind in the deposited material¹⁹. Keeping these in mind, an aqueous solution of $\text{SnCl}_4 \cdot 2\text{H}_2\text{O}$ is used as the precursor solution for spray pyrolysis.

2. Experimental techniques

Pure SnO_2 thin films were deposited onto microscopic glass substrates using the spray pyrolysis technique. The precursor of $\text{SnCl}_4 \cdot 2\text{H}_2\text{O}$ (0.2 M) was dissolved separately in a solution containing deionized water in proper ratio. This solution was mixed and sprayed onto the microscopic glass substrates at a substrate temperature of 350°C . The substrates were first cleaned with a water bath, followed by dipping in concentrated HCl, acetone and ethanol successively. Finally the substrates were rinsed in deionized water and allowed to dry in a hot air oven. In the spray unit, the substrate temperature was maintained with the help of heater, controlled by a feedback circuit. During spray, the substrate temperature was kept constant. Spray head and substrate heater kept inside a chamber, provided with an exhaust fan for removing gaseous by-products and vapors from the solvent. The values of deposition parameters like solution flow rate, carrier gas pressure and nozzle to substrate distance were kept as 2 ml/min, 1.5 bar and 20 cm, respectively (Table 1). A uniform coating on the substrate is achieved. Following deposition, the film was allowed to cool slowly to room temperature and washed with distilled water and then dried. The spray pyrolysis system used is as shown in Fig. 1.

Table 1. Process parameters for the spray deposition of the thin films.

Spray parameters	Optimum value/item
Nozzle	Glass
Nozzle-substrate distance	25 cm
$\text{SnCl}_4 \cdot 2\text{H}_2\text{O}$ solution concentration	0.1 M
Solvent	Distilled water
Solution flow rate	5 mL/min
Carrier gas	Compressed air
Substrate temperature	350°C

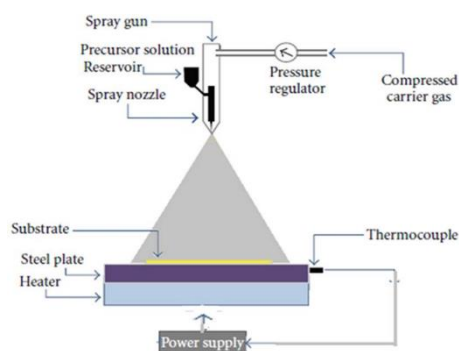


Fig. 1. The scheme of the spray pyrolysis setup.

2.1. Characterization

The deposited SnO_2 thin films were characterized by X-ray diffraction (XRD) pattern using $\text{CuK}\alpha$ radiation with $\lambda = 1.5418 \text{ \AA}$ (Rigaku III model). The scanning electron microscopy (FESEM, Hitachi S-4800) is employed to analyze morphology and microstructure. The elemental analysis (EDX) was studied using TESCAN SEM-VEGA III and CONTEXT software. The percentage of component elements was determined by the energy dispersive X-ray analysis (EDX) technique. Infrared spectra were obtained using Fourier transform infrared spectroscopy (FTIR,

Nicolet 6700) in the range from 400 to 4500 cm^{-1} . UV–Vis spectrum was recorded in the range of 300–1100 nm using a VARIAN CARY 5E spectrometer.

3. Result and discussion

3.1. Powder XRD analysis

The XRD patterns of deposited pure SnO_2 thin film are shown in Fig. 2. All of main diffraction peaks are indexed as the tetragonal rutile phase based upon JCPDS card no: 41-1445. The XRD patterns of deposited SnO_2 thin film are shown polycrystalline phases with determined h, k, l Miller indices of planes (110), (101), (200), (211), (220), (310), (301), and (321) corresponding to peak positions 26.793, 34.073, 38.0856, 51.9303, 54.871, 61.997, 66.090 and 78.806, respectively, as listed in Table 2.

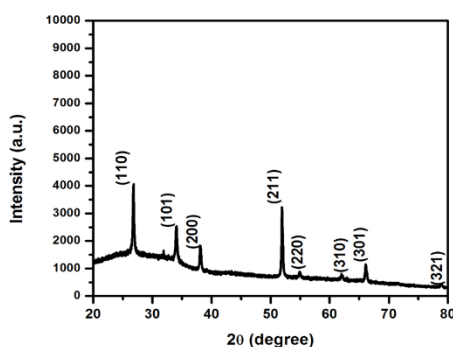


Fig. 2. X-ray diffraction pattern of pure SnO_2 thin film.

Table 2. The average crystallite size of pure SnO_2 thin films.

(h k l) planes	Angle, 2θ (degree)	d spacing (Å)	FWHM	Crystallite size (nm)
(110)	26.793	3.3248	0.204	41.83
(101)	34.073	2.6292	0.271	32.04
(200)	38.0856	2.36088	0.243	36.14
(211)	51.9303	1.75937	0.264	34.97
(220)	54.871	1.6718	0.27	34.64
(310)	61.997	1.4957	0.25	35.87
(301)	66.090	1.41261	0.227	39.61
(321)	78.806	1.2135	0.26	47.33

The average crystallite size is determined using by Debye–Scherrer’s formula with respect to peak plane²⁰.

$$\text{Crystallite size } D = 0.9\lambda/\beta\cos\theta \quad (1)$$

where D is the average crystallite size, λ is the wavelength X-ray diffracted, and $k = 0.98$ which is Scherrer’s constant, θ is the angle of diffraction and β is the full width at half maximum (FWHM) in radians. The crystal structure of SnO_2 thin film is cassiterite with the average crystallite size 37.80 nm.

3.2. Morphological analysis

The SnO₂ thin films deposited on glass substrate at 0.1 M solution concentrations. The surface morphology (FESEM) studies are shown in Fig. 3. It is observed that the film reveal a smooth surface, also some irregular pore shaped grains and can be seen which are as imbedded in the clusters²¹. This reveals that the film is uniform and forces to believe on the uniform distribution of larger number of small nuclei and agglomeration of these nuclei to form cluster. In this thin film lot of irregular grains with irregular shapes was found.

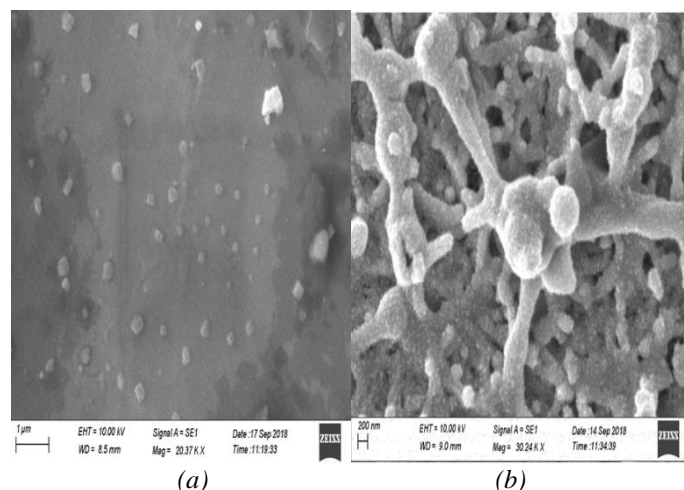


Fig. 3. SEM micrograph of pure SnO₂ thin film at different spots (a–b) and with different magnifications.

3.3. EDX analysis

The chemical composition elements of SnO₂ thin film are shown in Fig. 4. The EDX analysis products thin film exhibited the presence of Sn and O only. Expected stoichiometrically at% of Sn and O is 33.3 and 66.7 and observed at% of Sn and O is 39.58 and 60.42, respectively, which shows that the SnO₂ thin film is near to the stoichiometric compound.

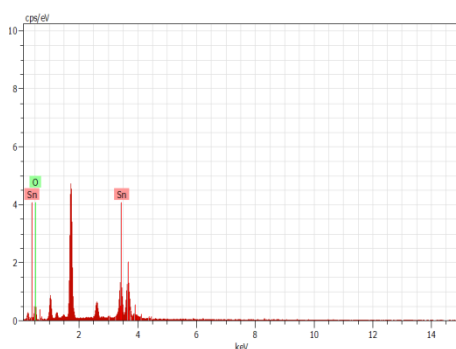


Fig. 4. EDX pattern of pure SnO₂ thin film.

3.4. FTIR Analysis

Pure SnO₂ thin film Fourier transform infrared spectra are shown in Fig. 5. The minimum transmittance on the wavelength range 3400–3500 cm⁻¹ is corresponding to the O–H bond stretching vibration of water molecules adsorbed²². The minimum transmittance in the range of 2300–2400 cm⁻¹ is produced by carbon dioxide. So by exposing the atmosphere and absorb carbon dioxide molecules are formed²². The wavelength ranges between 1600 and 1700 cm⁻¹ is related to

flexural vibrations. The minimum transmittance in the range of 400–700 cm^{-1} causes vibration of Sn–O–Sn and Sn–O in SnO_2 molecule^{23, 24}.

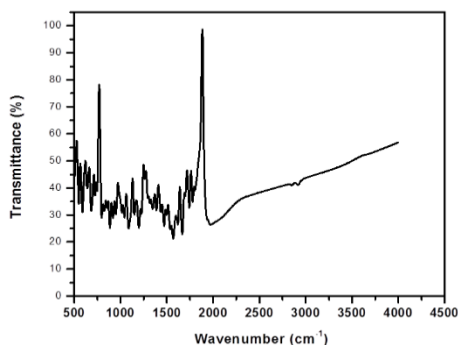


Fig. 5. FTIR spectra of pure SnO_2 thin film.

3.5. UV analysis

The absorption spectra of pure SnO_2 thin films are shown in Figs. 6 and 7. Considering the blue of the absorption positions from the bulk SnO_2 , the absorption onsets of the present samples can be assigned to the direct transition of electron in the pure SnO_2 thin films.

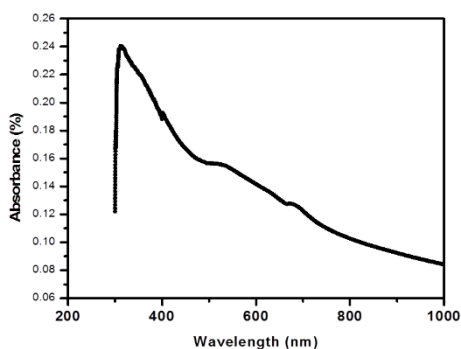


Fig. 6. Optical absorbance spectra pure SnO_2 thin films.

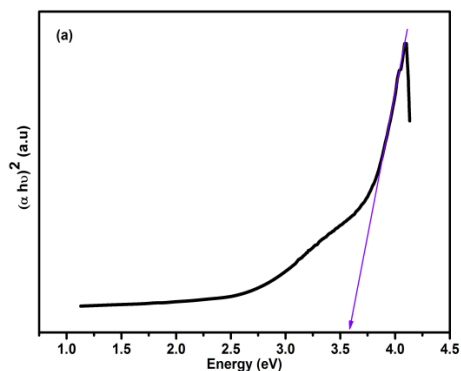


Fig. 7. The band gap energy of the pure SnO_2 thin films.

The absorption coefficient (α) was determined from the transmission spectra using the following equation²⁵:

$$\alpha = 1/t \ln(1/T)$$

where t is the film thickness and T is the optical transmission. The optical band gap energy (E_g) of the corresponding samples is determined by the Tauc plot equation:

$$\alpha(h\nu) = A (h\nu - E_g)^n,$$

where, E_g is the optical band gap, α is an absorption coefficient, h is Planck constant, A is a constant relative to the semiconductor material and 'n' is a value that depends on transition ($n = 2$ for direct band gap, $2/3$ for indirect forbidden gap and $1/2$ for indirect band gap). ν is the frequency and $h\nu$ is the photon energy. Figure 7 represents the plot of $(\alpha h\nu)^2$ vs. photon energy for pure SnO_2 thin films.

The direct band gap (E_g) of our samples is measured from the absorption coefficient data as a function of wavelength using the following Tauc relation. By extrapolating the linear portions of the $(\alpha h\nu)^2$ vs photon energy plot, the optical energy band gap was found to be 3.57 eV. It is observed that obtained tin oxide has the optical band gap larger than the value for bulk SnO_2 ²⁶⁻²⁸. It is related with the structural defects and the oxygen vacancies.

4. Conclusions

Pure SnO_2 thin film was deposited by spray pyrolysis technique and the impact on their structural, and optical properties of SnO_2 was studied. XRD and EDX studies confirmed the presence of the SnO_2 crystal by replacing Sn^{4+} host ions without changing the tetragonal structure. The XRD pattern analysis showed a development of average crystallite size with SnO_2 thin film. FESEM studies reveal that lot of irregular grains with irregular shapes was found. The optical energy band gap was found to be 3.57 eV. The pure SnO_2 films make them useful for wider optoelectronic device and gas sensor applications.

References

- [1] O. Fouad, G. Glaspell, M. El-Shall, *Top Catal.* **47**, 84 (2008).
- [2] X. Song, L. Liu, *Sens. Actuators A* **154**, 175 (2009).
- [3] G. Hirata, J. Mc Kittrick, T. Cheeks, J. Siqueiros et al., *Thin Solid Films* **288**, 29 (1996).
- [4] A. Djuricic, A. Ng, X. Chen, *Prog. Quantum Electron.* **34**, 191 (2010).
- [5] Q. Kuang, Z. Y. Jiang, Z. X. Xie, S. C. Lin et al., *J. Am. Chem. Soc.* **127**, 11777 (2005).
- [6] W. W. Wang, Y. J. Zhu, L. X. Yang, *Adv. Funct. Mater.* **17**, 59 (2007).
- [7] S. Ito, Y. Makari, T. Kitamura, Y. Wada et al., *J. Mater. Chem.* **14**, 385 (2004).
- [8] A. M. Saleh, N. A. Bakr, Z. T. Khodair, *Dig J Nanomater Bios.*, **13(3)**, 603, (2018).
- [9] L. Segueni A. Rahal, B. Benhaoua, N. Allag, A. Benhaoua, M. S. Aida, *Dig J Nanomater Bios.*, **14(4)**, 923, (2019).
- [10] G. E. Patil, D. D. Kajale, V. B. Gaikwad, G. H. Jain, *ISRN Nanotechnol.* **5**, 275872 (2012).
- [11] V. Janakiraman, V. Tamilnayagam, R. S. Sundararajan, S. Sivabalan, B. Sathyaseelan *Chalcogenide Letters* **17(8)**, 405 (2020).
- [12] V. Janakiraman, V. Tamilnayagam, R. S. Sundararajan, S. Suresh, C. S. Biju, *J Mater Sci Mater Electron.* Doi 10.1007/s10854-020-04110-2.
- [13] S. D. Shinde, G. E. Patil, D. D. Kajale, V. B. Gaikwad et al., *J. Alloys Compounds* **528**, 109012.
- [14] C. Cobianu, C. Savaniu, P. Siciliano, S. Capone et al., *Sensors Actuators B* **77**, 496 (2001).
- [15] R. Rella, P. Siciliano, S. Capone, M. Epifani et al., *Sensors Actuators B* **58**, 283 (1999).
- [16] R. Larciprete, E. Borsella, P. De Padova, P. Perfetti et al., *Thin Solid Films* **323**, 291 (1998).
- [17] G. Sberveglieri, G. Faglia, S. Groppelli, P. Nelli, *Sensors Actuators B* **8**, 79 (1992).
- [18] R. Dolbec, M. A. El Khakani, A. M. Serventi, R. G. Saint-Jacques, *Sensors Actuators B* **93**, 566003.
- [19] G. E. Patil, D. D. Kajale, D. N. Chavan, N. K. Pawar et al., *Bull. Mater. Sci.* **34**, 1 (2011).

- [20] B. D. Cillity, *Elements of X-ray diffraction*. 2nd ed. Reading: Addison-Wesley, 1956.
- [21] B. Sathyaseelan, K. Senthilnathan, T. Alagesan, R. Jayavel et al., *Mater. Chem. Phys.* **124**, 1046 (2010).
- [22] W. Brzyska, *Polish J. Chem.* **75**(1), 43 (2001).
- [23] K. Nakamoto, *Infrared and Raman spectra of inorganic and coordination compounds*, 4th edn. Hoboken: John Wiley; 2009. p 183.
- [24] J. M. Gallardo-Amores, T. Armaroli, G. Ramis, E. Finocchio et al., *Appl. Catal. B* **22**, 249 (1999).
- [25] S. S. Roy, J. Podder Gilberto, *J. Optoelectron. Adv. M.* **2**, 1479 (2010).
- [26] A. R. Razeghizadeh, L. Zalaghi, I. Kazeminezhad, V. Rafee, *Iran J. Chem. Chem. Eng.* **36**, 5 (2017).
- [27] G. Suresh, R. Sathishkumar, I. Baskaran, B. Sathyaseelan et al., *Int. J. Nano Dimens.* **10**(3), 242 (2019).
- [28] B. Sathyaseelan, C. Anand, A. Mano, S. M. Javaid Zaidi et al., *J. Nanosci. Nanotechnol.* **10**, 8362 (2010).